

JWST Reveals a Likely Jellyfish Galaxy at $z = 1.156$

IAN D. ROBERTS,^{1,2} MICHAEL L. BALOGH,^{1,2} VISAL SOK,³ ADAM MUZZIN,³ MICHAEL J. HUDSON,^{1,2,4} AND
PASCALE JABLONKA⁵

¹*Department of Physics & Astronomy, University of Waterloo, Waterloo, ON N2L 3G1, Canada*

²*Waterloo Centre for Astrophysics, University of Waterloo, 200 University Ave W, Waterloo, ON N2L 3G1, Canada*

³*Department of Physics and Astronomy, York University, 4700 Keele Street, Toronto, ON M3J 1P3, Canada*

⁴*Perimeter Institute for Theoretical Physics, 31 Caroline St N, Waterloo, ON N2L 2Y5, Canada*

⁵*Laboratoire d'astrophysique, École Polytechnique Fédérale de Lausanne (EPFL), CH-1290 Sauverny, Switzerland*

ABSTRACT

We report the discovery of COSMOS2020-635829 as a likely jellyfish galaxy undergoing to ram pressure stripping in a (proto)cluster at $z > 1$. High-resolution imaging from the *James Webb Space Telescope* reveals a symmetric stellar disk coupled to a unilateral tail of star-forming knots to the south. We show that these extra-planar continuum sources are embedded within an ionized gas tail that is kinematically connected to the disk of COSMOS2020-635829. Likely representing the highest-redshift discovery of a ram pressure stripped ionized gas tail. The tail sources are characterized by extremely young stellar populations ($\lesssim 100$ Myr), have stellar masses of $\sim 10^8 M_\odot$, and star formation rates of $0.1\text{--}1 M_\odot \text{ yr}^{-1}$. This work reinforces the notion that ram pressure stripping can perturb group and cluster galaxies at $z > 1$ and likely contributes to environmental quenching even near Cosmic Noon.

1. INTRODUCTION

For approximately 50 years it has been known, at least to some degree, that the properties of galaxies in over-dense environments like galaxy groups and clusters differ systematically from those relatively isolated in the field. This dichotomy is reflected in a number of galaxy properties, but among the most studied is the over-abundance of red, quiescent satellite galaxies in dense environments (e.g. Dressler 1980; Postman et al. 2005; Blanton & Moustakas 2009; Peng et al. 2010; Wetzel et al. 2012; Wilman & Erwin 2012; Haines et al. 2015; Roberts & Parker 2017). This ‘environmental quenching’ of galaxies is strongest in the most-massive galaxy clusters with the fraction of quiescent galaxies approaching the field value for the lowest-mass galaxy groups (e.g. Kimm et al. 2009; Wetzel et al. 2012).

The origins of this quenching has been attributed to a suite of physical mechanisms that are unique to dense environments (see Cortese et al. 2021 for a recent review), the most commonly invoked being: the cessation of cold-gas accretion onto satellite galaxies (often referred to as ‘starvation’ or ‘strangulation’), either due to the high virial temperature of the group or cluster halo

or due to the circum-galactic medium being stripped off of the galaxy (e.g. Larson et al. 1980; Balogh et al. 1999; Peng et al. 2015); or the direct stripping of cold-gas from galaxies, either due to ram pressure stripping (RPS, Gunn & Gott e.g. 1972; Gavazzi e.g. 1978; Gavazzi & Jaffe e.g. 1987) or from tidal interactions with other group/cluster galaxies that can either directly strip material or tidally stir/heat gas making it more easily removed by ram pressure (e.g. Boselli & Gavazzi 2006; Mayer et al. 2006). It is likely that the effectiveness of these various environmental perturbations depends on the mass of the host halo. For example, ram pressure strength scales with the density of, and velocity relative to, the ICM as $\rho_{\text{ICM}} v^2$, and thus will be strongest in massive galaxy clusters. Conversely, tidal interactions and even galaxy mergers will be more common in lower mass groups where the typical orbital velocities are closer to the escape velocity for two interacting galaxies.

In the low-redshift Universe, a comprehensive understanding of the relative balance between different quenching mechanisms as a function of host environment is still elusive – but progress has been made. It is now clear that RPS plays an important role in quenching galaxies in galaxy clusters. This has been inferred through the need for short quenching times (e.g. Quilis et al. 2000; Muzzin et al. 2014), observed signatures of outside-in quenching (e.g. Cortese et al. 2012; Schaefer

et al. 2017; Finn et al. 2018; Owers et al. 2019; Schaefer et al. 2019; Morgan et al. 2024; Broderick et al. 2025), as well as the identification of so-called ‘jellyfish’ galaxies with one-sided tails of stripped interstellar medium that extend well beyond the main galaxy disk (e.g. Gavazzi & Jaffe 1987; Gavazzi et al. 2001; Chung et al. 2007; Poggianti et al. 2017; Boselli et al. 2018; Roberts et al. 2021b, 2022a; Ignesti et al. 2023). In lower mass galaxy groups, the picture is less clear. RPS certainly does occur in such halos (e.g. Bureau & Carignan 2002; McConnachie et al. 2007; Rasmussen et al. 2006; Hu et al. 2024; Roberts et al. 2024; Finn et al. 2025), but the frequency is lower (Roberts et al. 2021a). Even in the most-massive clusters, it is unlikely that ram pressure is responsible for stripping all (or even most) of the molecular gas in satellite galaxies (e.g. Zabel et al. 2022; Watts et al. 2023; Brown et al. 2023). Instead, quenching likely operates in conjunction with gas depletion (which is then not replenished) from star formation, both prior to galaxies reaching the inner regions of groups and clusters where RPS is efficient, and after gas disks are truncated by ram pressure in order to ‘finish off’ quenching. This has recently been framed as a ‘slow-then-rapid’ quenching paradigm where this interplay between starvation/strangulation and RPS drives the quenched fractions in low-redshift clusters (Wetzel et al. 2013; Maier et al. 2019; van der Burg et al. 2018; Roberts et al. 2019; Manuwal & Stevens 2023; Morgan et al. 2024; Broderick et al. 2025).

At higher redshift ($z \sim 1-2$), far less is known. It has been shown that cluster red sequences in excess of the field population are in place in dense environments at these redshifts (e.g. Muzzin et al. 2012; Cerulo et al. 2016; Old et al. 2020). This in and of itself implies that relatively short quenching timescales are needed given the limited time available for group/cluster formation and subsequent environmental quenching at high- z . Direct evidence for RPS at high-redshift is limited due to both the required sensitivity to detect the typically faint morphological signatures of RPS and the required angular resolution for spatially resolving them. Of the examples in literature, Noble et al. (2019) present marginally resolved molecular gas extensions in $z \sim 1.6$ cluster galaxies that may represent ram-pressure stripped tails. More recently, Xu et al. (2025) report molecular gas observations of galaxies in a $z = 2.51$ protocluster, at least three of which show some compelling evidence for one-sided tails, potentially driven by ram pressure.

The bulk of galaxies on the cluster red sequence at $z \sim 0$ ceased substantial star formation at $z \gtrsim 1-2$ (e.g. Kodama & Arimoto 1997; de Propris et al. 1999; Mancone et al. 2010). Thus a key avenue for understand-

ing the quenched population in the local Universe is to observe environmental quenching mechanisms, such as RPS, in action at high- z . In the local Universe, ionized gas tails are among the most frequently identified signatures of RPS (e.g. Yagi et al. 2010; Poggianti et al. 2017; Boselli et al. 2018), but to-date no examples of ram-pressure stripped ionized gas tails have been identified beyond $z = 0.7$ (Boselli et al. 2019). Identifying analogous galaxies at high-redshift (to the extent that they exist) must be a fruitful path for advancing our knowledge of environmental quenching. Currently the number of known, unquestionable examples of RPS at $z > 1$ is likely zero, and the number of strong candidates in the present literature is almost certainly < 10 . Any new identification of such objects is thus an important addition.

In this work we present COSMOS2020-635829, a new, strong candidate for a satellite galaxy at $z > 1$ undergoing active RPS. COSMOS2020-635829 is associated with a cluster-mass, X-ray detected overdensity and shows a one-sided collection of blue, extra-planar knots that are co-spatial with an ionized gas tail. This is among the strongest candidates for a jellyfish galaxy at $z > 1$, and if said interpretation is correct, the current highest redshift example of a ram-pressure stripped ionized gas tail as well extra-planar star formation.

The outline of the the paper is as follows. In Sect. 2 we introduce the data products used in this work, including broadband imaging (JWST, HST, Subaru) as well as spatially resolved spectroscopy (Gemini). In Sect. 3 we provide an outline of COSMOS2020-635829’s status as a jellyfish galaxy candidate based on rest-frame optical and near-IR imaging. In Sect. 4 we present the detection of an ionized gas tail to the south of COSMOS2020-635829 that is co-spatial with the observed rest-frame optical asymmetries. In Sect. 5 we present an analysis of the ongoing star formation in the extra-planar sources, presumed to be fueled by ram-pressure stripped gas. Finally, in Sects. 6 and 7 we discuss the key results from this work as well as make concluding remarks. Throughout, we assume a flat Λ CDM cosmology with $\Omega_M = 0.3$, $\Omega_\Lambda = 0.7$, and $H_0 = 70 \text{ km s}^{-1} \text{ Mpc}^{-1}$.

2. DATA

2.1. Broadband Imaging

Our primary imaging source for this work is publicly available, multi-band *James Webb Space Telescope* (JWST) imaging of the COSMOS field from the COSMOS-Web Survey (Casey et al. 2023; Franco et al. 2025). This is from COSMOS-Web Data Release 0.5 which includes $\sim 0.3 \text{ deg}^2$ of the COSMOS field in the NIRCам F115W, F150W, F277W, and F444W fil-

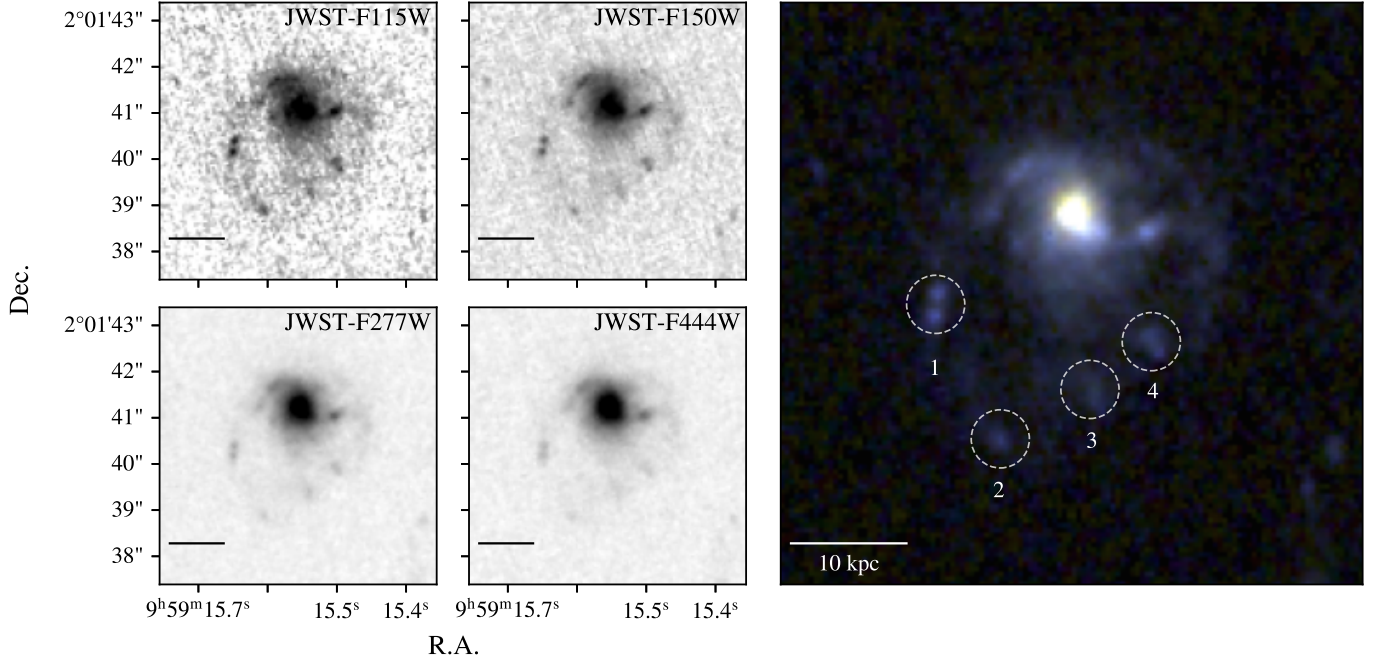


Figure 1. Thumbnail images of COSMOS2020-635829 for the 4 JWST filters used in this work. The RGB image on the right is a combination of the JWST F444W (red channel), the F277W (green channel), and F115W+F150W (blue channel). The dashed circles mark the four extra-planar sources that are identified in the tail of COSMOS2020-635829.

ters. A far smaller area is also covered by the MIRI F770W filter, though this does not cover COSMOS2020-635829. This JWST imaging was used to first identify COSMOS2020-635829 as a jellyfish galaxy candidate (see Sect. 3, Roberts et al. in prep). We also make use of *Hubble Space Telescope* (HST) F814W imaging (Koeke-moer et al. 2011) and deconvolved Subaru Suprime-Cam B-, V-, r -, and z -band imaging (Sok et al. 2022) in Sect. 5 for spectral energy distribution (SED) fitting. Finite-resolution deconvolution is applied to the deep Suprime-Cam imaging of the COSMOS field to achieve an angular resolution of $0.3''$, this procedure is described in detail by Sok et al. (2022).

2.2. GMOS Spectroscopy

We observed COSMOS2020-635829 with the GMOS IFU in the 2025A semester (PI: Roberts, program code: GN-2025A-FT-205). We used the single-slit GMOS IFU with a central wavelength of 8900 \AA (with $\pm 100 \text{ \AA}$ spectral dithers) and the R400 grating. This gives a field-of-view of $\sim 3.5'' \times 5''$ and a spectral resolution of $R = 3000$ ($\sigma_{\text{inst}} \simeq 43 \text{ km s}^{-1}$). Our main target is the redshifted [OII] $\lambda\lambda 3726 - 3729$ emission line doublet, which is among the brightest observable emission lines in the rest-frame optical spectrum. The $H\alpha$ line is not observable from the ground for COSMOS2020-635829 as it falls between the J and H atmospheric windows. We observed COSMOS2020-635829 for a total integration time of 5 h which was split over three nights (2025-

03-02, 2025-04-21, 2025-05-26) in observing blocks of $5 \times 1200 \text{ s}$, each bracketed by flat-field and CuAr arc observations. The standard star EG131 was also observed for spectrophotometric calibration. For the three nights the raw image-quality during our observations was 70th percentile, 70th percentile, 20th percentile, respectively, and the average airmass was 1.2, 1.5, 1.5.

Data reduction was done using the Gemini IRAF software package following the GMOS IFU-1 Data Reduction Tutorial. The standard reduction steps were completed, including bias and overscan correction, flat fielding, scattered light removal, cosmic-ray rejection, and sky subtraction. We use our standard star observation for flux calibration, and we further refine our flux scale using the calibrated DESI DR1 spectrum of COSMOS2020-635829. A calibrated data cube was produced for each 1200 s science exposure, with pixel sizes of $0.1''$ in the spatial directions and 0.76 \AA in the spectral direction. The cubes were then reprojected onto a common wavelength grid and coadded with inverse-variance weighting to produce our final science cube. In the vicinity of the [OII] doublet, we achieve a 1σ sensitivity of $\lesssim 10^{-18} \text{ erg s}^{-1} \text{ cm}^{-2} \text{ \AA}^{-1} \text{ arcsec}^{-1}$. We detect the [OII] line across the area of COSMOS2020-635829 and we do not detect the stellar continuum (nor did we expect to).

3. COSMOS2020-635829: A JELLYFISH GALAXY CANDIDATE AT $Z > 1$

COSMOS2020-635829 is an intermediate mass ($M_{\text{star}} \sim 10^{10} M_{\odot}$), strongly star-forming ($\text{SFR} \sim 100 M_{\odot} \text{ yr}^{-1}$) galaxy at a redshift of $z_{\text{spec}} = 1.1560$ (Weaver et al. 2022; DESI Collaboration et al. 2024). It was initially flagged as a RPS candidate galaxy by Roberts et al. (in prep) based on high-resolution rest-frame optical and near-IR imaging from the JWST COSMOS-Web survey (Casey et al. 2023). This selection of ram pressure candidates at $z \gtrsim 1$ will be outlined in detail by Roberts et al. (in prep), but in brief, galaxies were selected as ram pressure candidates according to one or more of the following morphological features.

1. A one-sided extension in the stellar distribution, which is interpreted as being in the direction of a potential ram pressure stripped tail. This extension may be associated with unwinding spiral arms (e.g. Bellhouse et al. 2021), but it does not need to be.
2. A one-sided collection of knots that are detached from the main stellar distribution of the galaxy. We require that these knots are similar in color to at least some part of the main galaxy, in order to reduce the odds of background sources in projection.
3. Evidence for enhanced star formation on the proposed leading edge. We require this to be in conjunction with a proposed tail direction from one of the above features. This means that a galaxy that shows apparently asymmetric star formation within its disk, but no sign of a one-sided extension, will not be classified as a ram pressure candidate. Signs of enhanced star formation on the leading edge may be used to classify a galaxy as a ram pressure candidate with only marginal evidence for a ‘tail’ extension, if the orientation of the potential enhanced star formation and tail direction are mutually consistent.

This is analogous to the visual selections of ram pressure candidates that has become relatively common, and quite successful, at $z \sim 0$ (Ebeling et al. 2014; Poggianti et al. 2016; Roberts & Parker 2020; Durret et al. 2021; Roberts et al. 2022b; Crossett et al. 2025). In this framework the direction of the one-sided extension is interpreted as the direction of a *potential* ram pressure tail. We stress that these visual selections will by no means identify a pure sample of galaxies undergoing RPS, as there are other physical processes (e.g. tidal effects) that can perturb galaxies in groups and clusters, but through follow-up observations and analyses we can hope to confirm some fraction of these candidates.

In Fig. 1 we show single-band images of COSMOS2020-635829 in the four COSMOS-Web filters as well as a color-composite. The morphology of COSMOS2020-635829 is given by a symmetric main galaxy component coupled to compact, relatively blue, knots distributed to the south of the galaxy. It is these knots for which COSMOS2020-635829 was selected as a ram pressure candidate under the assumption that they may correspond to sites of extra-planar star formation within a ram pressure stripped gaseous tail (i.e. criterion #2). These four detached sources are highlighted in the color composite in Fig. 1 and will be the subject of further investigation in Sect. 5.

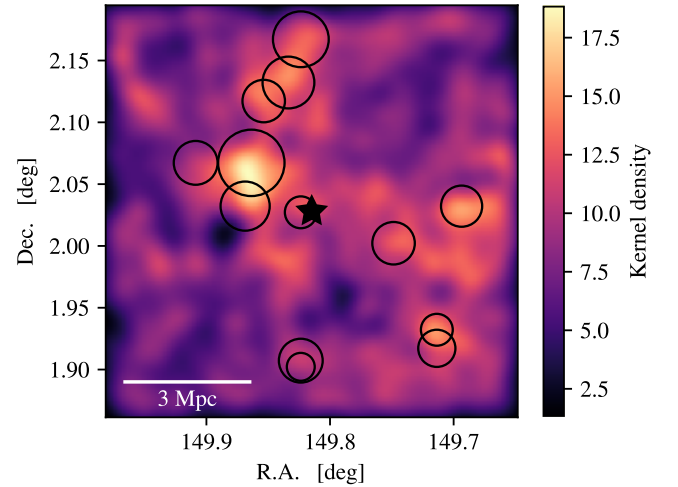


Figure 2. Large scale structure around COSMOS2020-635829. The large star marks the position of COSMOS2020-635829. The colormap shows a 2D kernel density estimate of all galaxies from the COSMOS2020 catalog within 10 arcminutes of COSMOS2020-635829 and with $1.0 < z_{\text{phot}} < 1.3$. Open circles correspond to groups/clusters from AMICO-COSMOS catalog within 10 arcminutes of COSMOS2020-635829 and with $1.0 < z_{\text{phot}} < 1.3$.

The ram pressure candidates from Roberts et al. (in prep) are selected without knowledge of the environments within which the galaxies reside, but it is found post classification that the identified ram pressure candidates are preferentially associated with overdense environments. COSMOS2020-635829 is no exception. In Fig. 2 we show the 2D galaxy density distribution for galaxies within 10' of COSMOS2020-635829 and with $1.0 < z_{\text{phot}} < 1.3$. COSMOS2020-635829 is associated with a complex and extended overdensity. The galaxy is spatially coincident with a $\sim 2 - 3 \times 10^{13} M_{\odot}$ halo at $z_{\text{phot}} \sim 1.23$, as identified by the AMICO cluster finding algorithm (Toni et al. 2024). This halo also appears at the outskirts of a strong galaxy overdensity centered on two halos in the AMICO-COSMOS catalog with photo-

z 's of 1.15 and 1.29, each X-ray detected at $\sim 4\sigma$, and with a combined halo mass of $\sim 10^{14} M_{\odot}$.

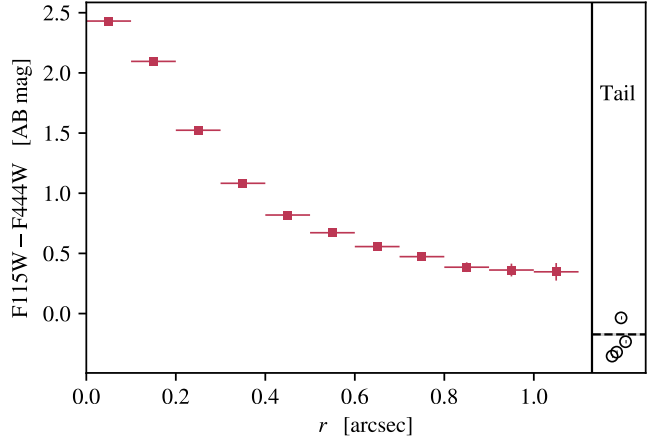
The closest galaxy companion to COSMOS2020-635829 (with $1.0 < z_{\text{phot}} < 1.3$) has a projected separation of ~ 75 kpc (Weaver et al. 2022). While we cannot fully rule out a tidal origin for the observed morphology of COSMOS2020-635829, this shows that it does not currently have any close tidal companions. There is always the possibility of a past tidal interaction with a satellite that is no longer in the vicinity of COSMOS2020-635829. Stellar tidal tails should have colors that are similar to the host galaxy, particularly the outskirts of the host galaxy where stars are most easily unbound. In Fig. 3 we plot the F115W–F444W color profile¹ for the main disk of COSMOS2020-635829 compared to the tail (both for individual sources and integrated over tail region). The color profile is extracted in $0.1''$ circular annuli from the galaxy center out to the edge of the disk ($\sim 1''$). The color of the tail is clearly bluer than all regions of the main disk, thus inconsistent with the stellar emission in the tail resulting from simple tidal stripping. We cannot rule out the possibility that gas is tidally stripped from COSMOS2020-635829 which then proceeds to form stars in situ in the tail, but gas being tidally stripped without strongly distorting the stellar distribution seems unlikely. Conversely, a stellar tail which is bluer than the main galaxy is exactly what is expected from star formation within a ram pressure stripped tail.

Given the one-sided nature of the observed asymmetries in both stars and gas (see next section), the relatively undisturbed morphology of the main stellar disk, and the color difference between the tail and the galaxy outskirts, we favor a ram pressure origin for these perturbations and will proceed, primarily, under this presumption for the remainder of the paper.

4. DETECTION OF AN IONIZED GAS TAIL

The association with an overdense environment is a necessary but not sufficient condition for establishing COSMOS2020-635829 as a jellyfish galaxy undergoing RPS. Furthermore, the detached knots in the JWST imaging of COSMOS2020-635829 cannot be definitively associated with the main galaxy through photometry alone. In this section we present the detection of an ionized gas tail to the south of COSMOS2020-635829, spatially coincident with the detached rest-frame optical/near-IR sources.

¹ We note that the qualitative trends seen in Fig. 3 are not sensitive to the choice of filters for the plotted color.



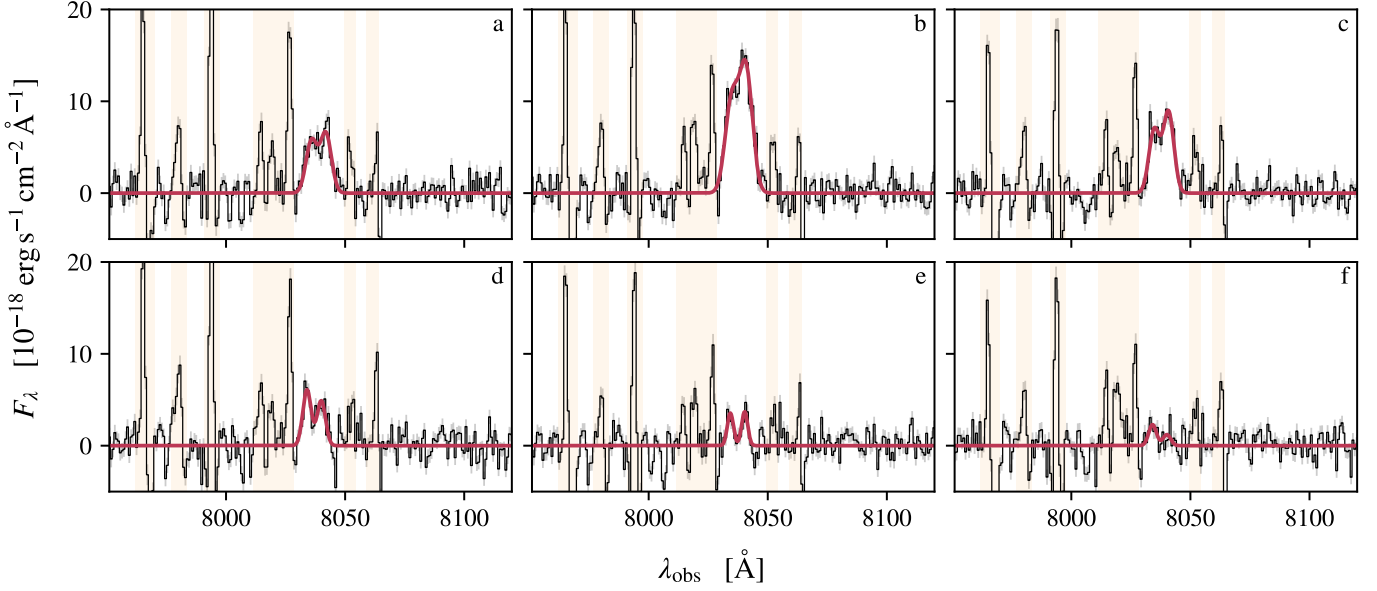


Figure 5. Extracted spectra around the [OII] line for various slices along the tail axis. The labels in each panel correspond to the aperture labels in Fig. 4. The black line and shading show the observed spectrum and uncertainty and the red line shows the best-fit double Gaussian model. These spectra are shown post continuum subtraction with a first-order polynomial. The yellow bands mark regions of the spectrum where significant sky-line residuals are seen, these regions of the spectrum are masked during fitting.

We also show 6 apertures along the tail axis, labeled ‘a’ through ‘f’, which have widths of $2.5''$ and heights of $0.75''$. The height of $0.75''$ corresponds to the FWHM image quality ($\sim 0.7'' - 0.8''$) and the width of $2.5''$ is chosen to span the full optical disk of COSMOS2020-635829. A key goal of the GMOS IFU observations of COSMOS2020-635829 is to test for the presence of an ionized gas tail that is co-spatial with the inferred ram pressure tail from broadband imaging. To do so we extract spectra around the [OII] $\lambda\lambda 3726 - 3729$ lines for each aperture along the tail axis. If a stripped ionized gas tail is present then we should see [OII] emission that extends beyond the main optical disk of the galaxy (radius $\sim 1''$), and specifically this should be seen to the south of COSMOS2020-635829.

Fig. 5 show these extracted spectra. We fit each spectrum with a model that is a composite of a continuum model and a double-Gaussian model for the [OII] doublet, given by

$$F_{\lambda}(\lambda) = P(a_0, a_1, \lambda) + \mathcal{N}(A_1, v, \sigma, \lambda) + \mathcal{N}(A_2, v, \sigma, \lambda), \quad (1)$$

where λ is the observed wavelength, P is a first-order polynomial to account for any offset or tilt in the continuum level, and \mathcal{N} are normal distributions with peak fluxes A_1 and A_2 corresponding to the two [OII] lines. We tie both lines in the [OII] doublet to a common velocity (v) and linewidth (σ). We also set a physically motivated prior range of $0.35 < A_2/A_1 < 1.5$ for the flux ratio between the two [OII] lines (Copetti & Writzl

2002; Pradhan et al. 2006). For each extracted spectrum this gives six free parameters. We determine the best-fit parameters using the Markov-Chain Monte Carlo package EMCEE (Foreman-Mackey et al. 2013) with flat priors on all model parameters. Chains are all checked for convergence by ensuring that the number of samples is greater than 50τ , where τ is the chain autocorrelation time (see EMCEE documentation).

The best fit spectral models are shown in Fig. 5 in red. We note that the observed spectra and best-fit model in Fig. 5 have had the best-fit continuum polynomial subtracted off. The yellow bands in the panels mark regions of the spectra that are masked during fitting due to significant residuals from sky line subtraction. We calculate the total [OII] flux as

$$F_{[\text{OII}]} = \sqrt{2\pi}\sigma(A_1 + A_2). \quad (2)$$

We detect the [OII] doublet in all apertures. This includes detections at separations well beyond the main stellar disk and even beyond the extra-planar sources seen in the JWST imaging. In Fig. 6(top) we plot [OII] flux as a function of distance from the galaxy center (dy) in kiloparsecs. We consider the flux profile shown in Fig. 6 to be indicative of a detected ionized gas tail to the south of COSMOS2020-635829. The ionized gas emission extends beyond the optical galaxy disk by ~ 20 kpc all the way to the edge of the IFU field-of-view. For reference, in Fig. 6(top) we overplot the best-fit Sérsic profile fit to the F277W image of COSMOS2020-635829

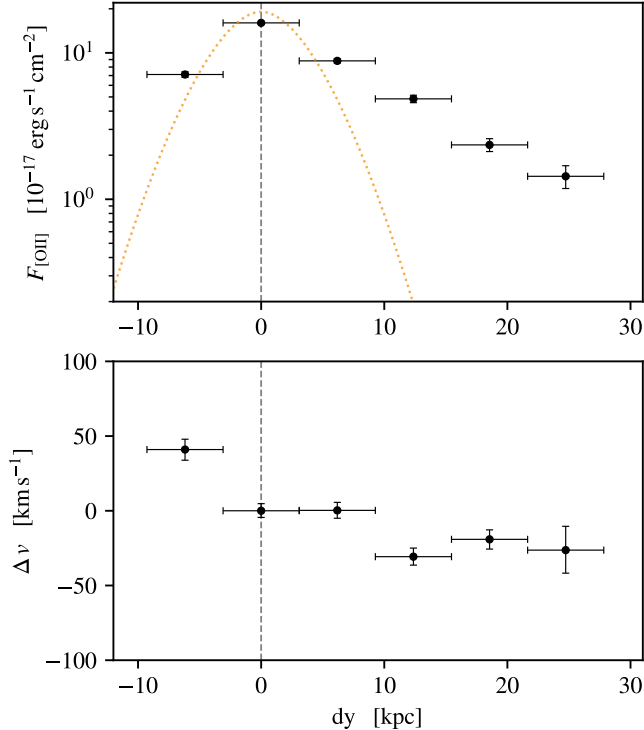


Figure 6. Profiles of [OII] flux (top) and velocity (bottom) along the tail axis, the dashed vertical line marks the center of the galaxy. The y -errorbars correspond to the 16th and 84th percentiles from the posterior distributions for the spectral fits. The x -errorbars correspond to the aperture width (see Fig. 4). For reference, the orange dotted line shows the best-fit Sérsic profile for the main disk of COSMOS2020-635829, which has been scaled arbitrarily to match the normalization of the [OII] profile. The velocity profile has been normalized such that $v = 0$ corresponds to the galaxy center.

(after convolution to the resolution of the GMOS spectroscopy), which we arbitrarily shift the normalization of to match that of the [OII] profile. This reflects the symmetric component of the galaxy disk and highlights the excess [OII] emission that is present for $dy \gtrsim 10$ kpc.

In Fig. 6(bottom) we show the velocity profile for the detected ionized gas along the tail axis. A clear velocity gradient is observed from the the leading side through to the far edge of the tail. This coherence definitively associates this extra-planar ionized gas emission with the main galaxy. It also indirectly indicates that the extra-planar broadband optical/near-IR (rest frame) emission to the south of COSMOS2020-635829 is also associated with the main galaxy.

5. EXTRA-PLANAR STAR FORMATION

Given the spatial coincidence between the ionized gas tail and the detached JWST sources, and given the kinematic association between ionized gas tail and the main

Table 1. Properties of tail regions

ID	R.A.	Dec.	$\log_{10}(M_{\star}/M_{\odot})$	$\text{SFR}/M_{\odot} \text{ yr}^{-1}$
1	149.81521	2.02786	$8.3^{+0.2}_{-0.4}$	$0.46^{+0.19}_{-0.12}$
2	149.81502	2.02747	$8.0^{+0.2}_{-0.3}$	$0.25^{+0.12}_{-0.09}$
3	149.81476	2.02761	$8.3^{+0.1}_{-0.2}$	$0.36^{+0.23}_{-0.11}$
4	149.81459	2.02775	$8.2^{+0.2}_{-0.2}$	$0.39^{+0.21}_{-0.13}$

galaxy, we believe that these extra-planar optical/near-IR sources reflect sites of in situ star formation in a ram-pressure stripped tail. In this section we estimate the properties of these star-forming knots via SED fitting. We measure photometry within the four apertures shown in Fig. 1. We note that ‘region 1’ (and arguably ‘region 4’) contains two peaks in the JWST imaging but we treat it as a single source since it is blended into a single source in the deconvolved Subaru imaging. The filters used are JWST F115W, F150W, F277W, and F444W, HST F814W, and Subaru B, V, r , and z . As mentioned in Sect. 2.1, we use the Subaru imaging from Sok et al. (2022) that is deconvolved to a resolution of $0.3''$ and prior to measuring fluxes we also convolve the JWST and HST imaging to this resolution. We only include filters in the SED fitting where the flux is detected in the source aperture at $>5\sigma$. We determine the flux uncertainty by randomly positioning 1000 apertures (of equal size to the source aperture) across the image and measuring fluxes. We take the flux error to be the sigma-clipped standard deviation of the resulting aperture flux distribution. We note that the deconvolved z -band flux is undetected for all four sources.

We perform SED fitting using the BAGPIPES code (Carnall et al. 2018, 2019) with the NAUTILUS sampler (Lange 2023). We assume a flexible continuity star formation history model and a Calzetti dust attenuation law (Calzetti et al. 2000). We use age bins of $[0, 30, 90, 650, 1800, t_{\text{max}}]$ Myr, where t_{max} is the age of the Universe at $z = 1.156$. These bins correspond to a minimal and maximal age bin with approximately logarithmic time-spacing in between. Dust A_V is allowed to vary freely between 0 and 2 and metallicity between 0.01 and 2.5 solar. We include a nebular emission component from CLOUDY (Ferland et al. 2017) with the ionization parameter fixed to $\log_{10}(U) = -3$ and fix the redshift to the spectroscopic redshift of COSMOS2020-635829.

In Fig. 7 we show the SEDs for each of the tail sources alongside the best-fit spectrum from BAGPIPES. Immediately by-eye it is clear that the photometry for all of the tail sources is consistent with a very young stellar popu-

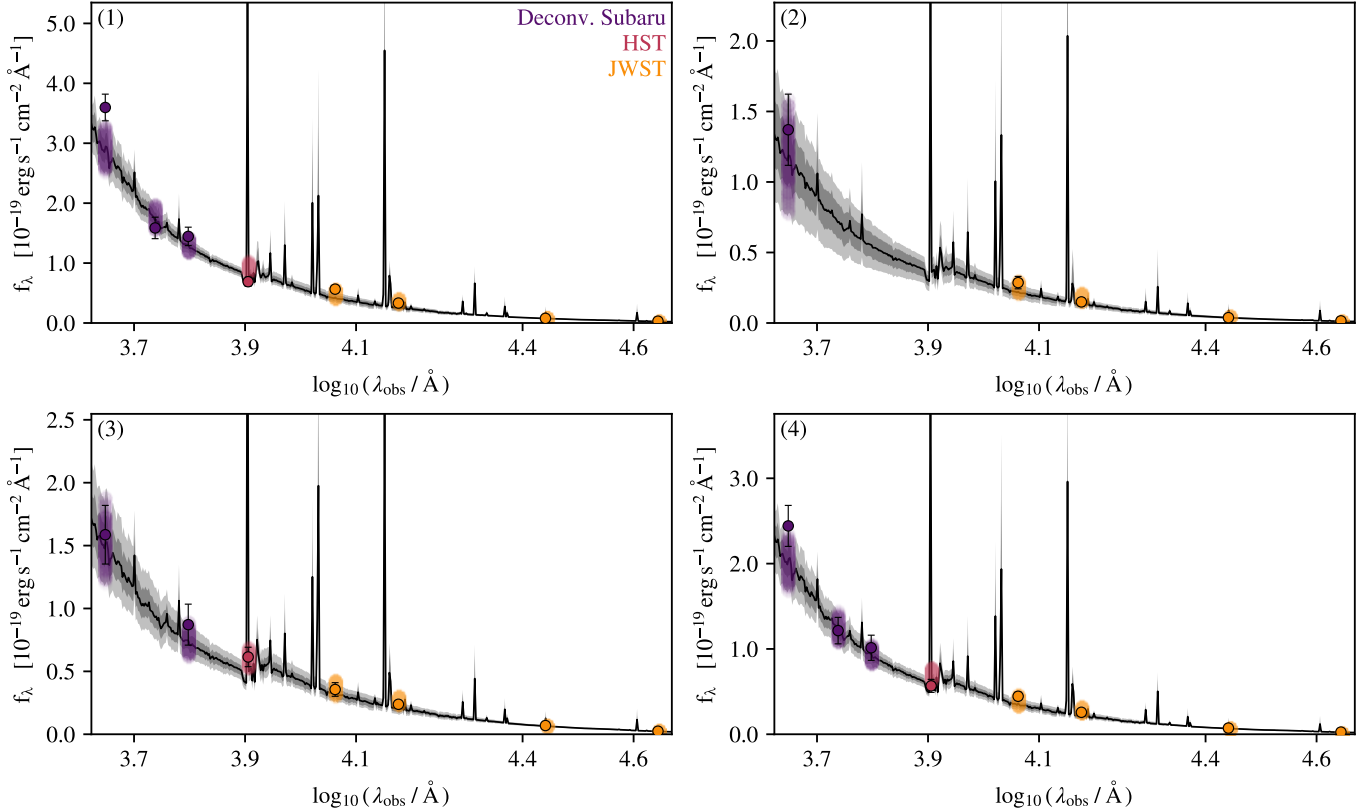


Figure 7. BAGPIPES SED fits for the four extra-planar sources identified in the tail of COSMOS2020-635829. Observed fluxes are shown by the data points. The solid black line shows the best-fit spectrum (50th percentile) and then gray shaded regions show the 68% and 95% credible regions. The colored bands show the 95% credible region for the expected flux in each of our observed filters, given the fitted model spectra. The region number (see Fig. 1) is listed in the upper-left corner.

lation, both by the lack of a significant Balmer break and the steep UV slope. This is reinforced quantitatively in Fig. 8 where we show the binned star formation histories from the SED fits. All sources are consistent with star formation exclusively within the past 100 Myr. The derived star formation rates and stellar masses for each of the tail sources are listed in Table 1, where the listed SFRs correspond to averages over the past 100 Myr. Stellar masses are generally around $10^8 M_{\odot}$ with SFRs that are a few tenths of a solar mass per year.

For further reference we also derive an integrated SFR for the main disk of COSMOS2020-635829 via SED fitting following the same procedure and using the same filters as for the tail sources (though the galaxy disk is detected in z -band). We measure photometry for the disk in an aperture centered on the galaxy center with a diameter of $2.5''$, which was determined by-eye to correspond to the size of the main disk (see, for example, Fig. 4), though this is also consistent with the size derived from Sérsic fitting in Sect. 4. We estimate a log stellar mass (in solar masses) of $10.16^{+0.13}_{-0.08}$ and a SFR of $89^{+51}_{-54} M_{\odot} \text{ yr}^{-1}$. These are consistent with the COSMOS2020 values of $10.30^{+0.05}_{-0.07}$ and 71^{+22}_{-14} (Weaver et al.

2022). This means that the tail sources individually account for ~ 1 – 2% of the stellar mass of the main disk and $\sim 0.5\%$ of the SFR (averaged over the past 100 Myr).

6. DISCUSSION

In this work we present evidence for the first ram-pressure stripped ionized gas tail at $z > 1$, which is found trailing to the south of the starburst galaxy COSMOS2020-635829 at $z = 1.156$. We also constrain for the first time the strength of extra-planar star formation in a ram-pressure stripped tail at these redshifts. While there are no direct comparisons for COSMOS2020-635829 at $z > 1$, we can compare the observed properties of COSMOS2020-635829 to jellyfish galaxies at lower redshift.

We first address the plausibility of RPS given the overdensities that COSMOS2020-635829 appears associated with (see Fig. 2). The smaller ($\sim \text{few} \times 10^{13}$) halo centered directly on COSMOS2020-635829 is, at best, marginally detected in X-rays with a luminosity of $8 \pm 6 \times 10^{42}$, so while it may support a dense ICM we cannot say for sure. The large overdensity to the north-east of COSMOS2020-635829 has an X-ray luminosity

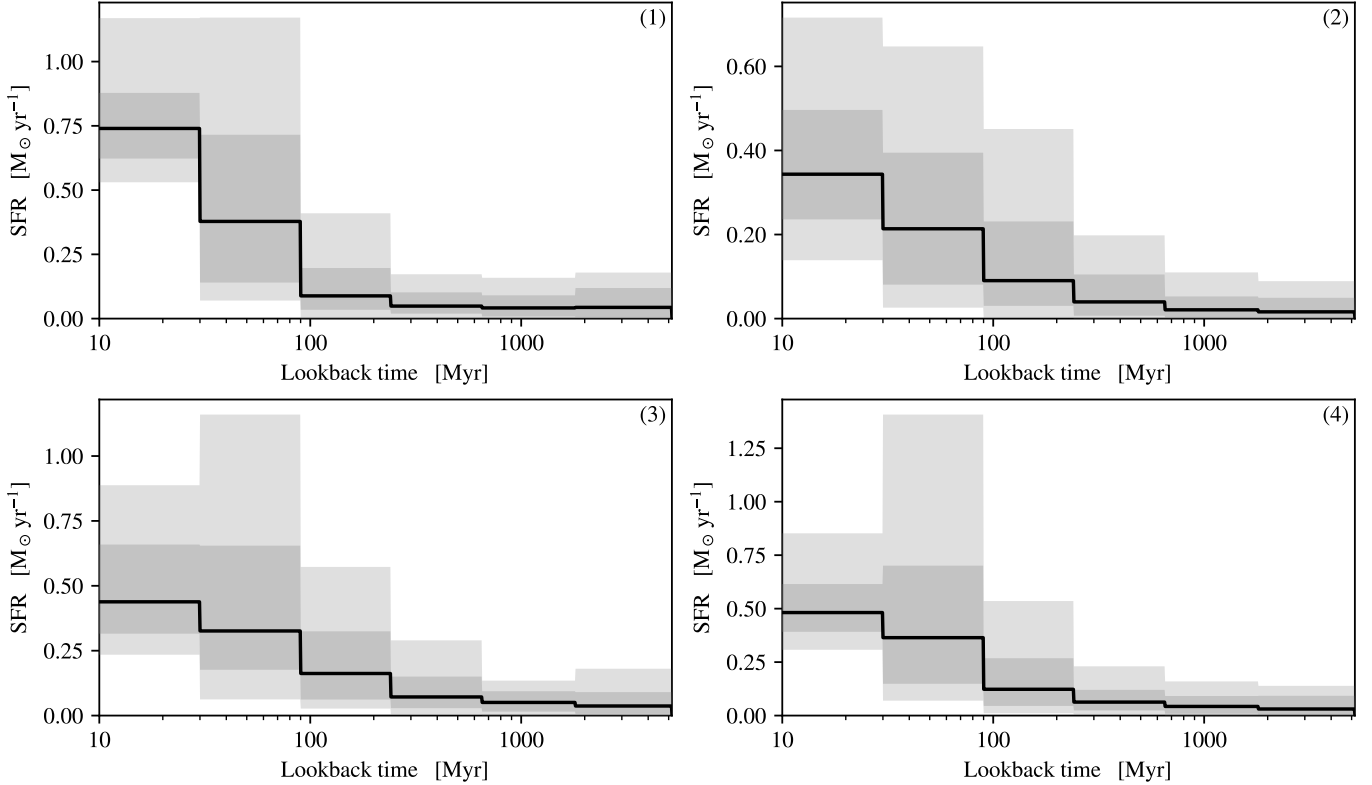


Figure 8. Star formation histories for the four extra-planar sources in the tail of COSMOS2020-635829. Star formation histories are determined from the SED fits shown in Fig. 7. We use a flexible star formation history model with six logarithmically-spaced age bins between 0 and ~ 5 Gyr. The solid black line corresponds to the median star formation history and the shaded bands show the 84th and 95th percentile credible regions.

of $2 \pm 0.5 \times 10^{43} \text{ erg s}^{-1}$ (Toni et al. 2024) detected at 4σ . This X-ray luminosity is not dissimilar from values for massive groups and low-mass clusters at $z \sim 0$ (e.g. Sun 2012). Based on this X-ray luminosity we obtain an order of magnitude estimate for the corresponding ICM density of $\sim 10^{-26} \text{ g cm}^{-3}$, which is likely reflective of the inner regions of the halo. Even if the ICM density falls off by one or two orders of magnitude towards the outskirts of the halo, this still gives possible ram pressure strengths of $\sim 10^{-11} - 10^{-13} \text{ g cm}^{-1} \text{ s}^{-2}$ for galaxy velocities between a few hundred and a thousand kilometers per second. These ram pressure strengths are similar in magnitude to values estimated from observations of RPS in the local Universe and from hydrodynamic simulations (e.g. Gunn & Gott 1972; Steinhauser et al. 2016; Jaffé et al. 2018; Roberts et al. 2019; Yun et al. 2019; Broderick et al. 2025). Thus based on the X-ray data available for this system, there is no reason to exclude RPS as a perturbing force for COSMOS2020-635829. In fact, assuming that ICM profiles remain self-similar out to $z > 1$ (McDonald et al. 2017), then the strength of ram pressure (at fixed group/cluster mass) at these redshifts should be as strong, if not stronger, than at $z \sim 0$ (given the evolution in the critical density of the Uni-

verse). At some point this self-similarity likely breaks down at epochs where the ICM is still in the process of formation, though what redshift range this corresponds to is still uncertain.

At lower redshift, Boselli et al. (2019) detect striking 50–100 kpc ram-pressure stripped [OII] tails behind two satellite galaxies in a $\sim 10^{14} M_{\odot}$ cluster at $z \sim 0.7$. Boselli et al. find a typical [OII] surface brightness in the stripped tails of a few times $10^{-18} \text{ erg s}^{-1} \text{ cm}^{-2} \text{ arcsec}^{-2}$, whereas we find a typical [OII] surface brightness of $\sim 10^{-17} \text{ erg s}^{-1} \text{ cm}^{-2} \text{ arcsec}^{-2}$. The observed size of tail that we detect is far shorter than the tails found by Boselli et al. (2019), though for galaxy 345 in Boselli et al. the [OII] surface brightness within 10–20 kpc of the galaxy disk is close to the typical value that we find for COSMOS2020-635829. This may suggest that the intrinsic length of the ionized gas tail behind COSMOS2020-635829 is much longer than we observe, but this will require significantly deeper observations to constrain. At lower redshift, the largest compilation of [OII] detected ram-pressure stripped tails is Moretti et al. (2022) with ~ 10 RPS galaxies in the A2744 and A370 clusters at $z \sim 0.3$ – 0.4 . A new revelation from Moretti et al. is the fact that the ram-pressure

tails in their sample show exceptionally high [OII]-to-H α ratios relative to the typical values for galaxy disks. They argue that this anomalous ratio is either driven by the low gas densities in ram pressure tails or is due to the complex interaction between the stripped tail and the surrounding ICM. At $z = 1.156$, the H α line falls between the J- and H-bands and is thus unobservable from the ground for COSMOS2020-635829. So while we do not have constraints on the H α emission for COSMOS2020-635829, these high [OII]-to-H α ratios seen at intermediate redshifts may be aiding our ability to detect [OII] in the tail of COSMOS2020-635829 at $z > 1$. Moving forward, constraints on the H α emission from COSMOS2020-635829 and its stripped tail will require spectroscopy from space.

In Fig. 1 we highlight four extra-planar regions in the tail of COSMOS2020-635829 that are clear from the JWST imaging. We note that regions 1 and 4 are resolved into two sources in the JWST imaging but are blended into one in the deconvolved Subaru imaging that we use for SED fitting. These regions are blue in color and are consistent with exclusively young stellar populations formed within the past 100 Myr. Detached star-forming knots in Virgo cluster ram-pressure tails tend to have stellar masses of $\sim 10^3$ – $10^5 M_\odot$ and SFRs of $\sim 10^{-4}$ – $10^{-3} M_\odot \text{ yr}^{-1}$ (Hester et al. 2010; Fumagalli et al. 2011; Boselli et al. 2021; Junais et al. 2021; Boselli et al. 2022). For star-forming knots in the tails of jellyfish galaxies from the GASP survey (Gas Stripping Phenomena in galaxies with MUSE, Poggianti et al. 2017), stellar masses range between $\sim 10^6$ – $10^8 M_\odot$ and SFRs between $\sim 10^{-4}$ – $10^{-1} M_\odot \text{ yr}^{-1}$. These can be compared to the typical stellar masses of $\sim 10^8 M_\odot$ and SFRs of $\sim 0.3 M_\odot \text{ yr}^{-1}$ derived in this work for the four tail regions. These differences relative to the knots for Virgo galaxies is likely driven by the differences in physical resolution such that the JWST sources in regions in this work may correspond to multiple small sources blended together. Relative to $z \sim 0$, at $z \sim 1$ there is an increase by an order of magnitude in the normalization of the SFMS (e.g. Speagle et al. 2014) which may also manifest itself in the specific star formation rate of detached star-forming knots. Relative to GASP sources, the physical properties of the four tail regions in this work are roughly consistent with the most-massive GASP knots, though the SFRs for the regions in the tail of COSMOS2020-635829 are slightly larger (Poggianti et al. 2019). Incorporating the factor of ~ 10 evolution in the SFMS moves the sources from this work well within the scatter of the GASP sample, though it remains to be seen whether this factor applies to star formation in stripped tails.

We can speculate on the fate of these extra-planar star-forming knots observed at $z > 1$. They may remain bound to the dark-matter halo of COSMOS2020-635829 and eventually be re-accreted on to the disk. The radial velocity offset of the tail relative to the main galaxy is modest at $\lesssim 50 \text{ km s}^{-1}$, but we cannot say whether this is indicative of a modest 3D velocity offset or a larger 3D velocity offset that is primarily in the plane of the sky. Simulations of isolated RPS find that most stars formed within 20 kpc of the disk will eventually fall back onto the galaxy (Tonnesen & Bryan 2012; Akerman et al. 2025), which is about the maximum separation that we observe for tail sources from the disk of COSMOS2020-635829. Thus, at least based on simulations, this may be the most likely fate. Alternatively these knots are unbound from COSMOS2020-635829. In this scenario there are two broad possibilities: either they survive as some sort of compact stellar collection or they are tidally disrupted and disperse. The latter would contribute to the building up the intracluster light (ICL) that is observed in clusters from $z \sim 0$ out to $z \gtrsim 1$ (e.g. Lin & Mohr 2004; Jiménez-Teja et al. 2019; Burke et al. 2012; Joo & Jee 2023). Sect. 5 suggests that $\sim 10^8$ – $10^9 M_\odot$ of total stellar mass has formed in the wake of COSMOS2020-635829 over the past ~ 100 Myr. Exactly how much ICL could be built up in this fashion over the history of the cluster will depend enormously on the statistical frequency of RPS, and specifically extra-planar star formation in ram-pressure tails. Hydrodynamic simulations predict that up to 30% of the ICL is built-up by ‘intracluster star formation’ in gas clouds stripped from infalling galaxies (Puchwein et al. 2010), which is analogous to the extra-planar star formation that we measure for COSMOS2020-635829. However, some simulation results suggest that this extra-planar star formation plays a much smaller role in ICL accumulation (Tonnesen & Bryan 2012; Akerman et al. 2025). The other possibility is that these sources are self-gravitating and remain as bound objects that become separated from COSMOS2020-635829. Such objects would, by definition, be dark-matter deficient. This notion of small ‘galaxies’ forming within ram pressure tails is not a new one and has been speculated on both via the lens of low-redshift observations as well as hydrodynamic simulations (e.g. Poggianti et al. 2019; Lora et al. 2024). The masses of the tail sources in this work are consistent with the masses of dwarf galaxies in clusters at $z \sim 0$, but we have limited information on their sizes. The SED fits in Sect. 5 are done at $0.3''$ resolution (limited by the deconvolved Subaru images), but it is clear from JWST images in Fig. 1 that the continuum sizes of these sources are smaller than this. We

estimate intrinsic FWHM sizes for these tail sources of $\sim 0.13'' \approx 1$ kpc (see Appendix A), corresponding to effective radii of ~ 500 pc. Thus the size and stellar mass of continuum sources in the tail of COSMOS2020-635829 do coincide with typical values for dwarf galaxies in low- z clusters (e.g. Kormendy et al. 2009; Marleau et al. 2025), but the dynamical evolution of these sources from $z \sim 1$ to the present-day is highly uncertain. Even if they do survive as bound objects, which is far from a given, they may end up looking very different than they do at $z > 1$.

Finally, we briefly discuss the current evidence for RPS at $z > 1$, beyond this work. Xu et al. (2025) present compelling evidence for ram-pressure stripped molecular gas tails in a few galaxies² that are part of a $z = 2.51$ protocluster with a mass of $\sim 10^{14} M_{\odot}$. If confirmed, this would show that RPS is truly operating all the way back to Cosmic Noon. The galaxies from Xu et al. (2025) are broadly of a similar stellar mass and SFR to COSMOS2020-635829, and like this work, the proposed ram-pressure tails are shown to be kinematically connected to the main galaxy. We do not have molecular gas observations of COSMOS2020-635829, and Xu et al. (2025) do not have resolved rest-frame optical spectroscopy, so the direct comparisons are limited. That said, these works highlight the potential multiwavelength nature of ram-pressure tails at $z > 1$, a fact that is already well known in the low-redshift Universe (e.g. Chung et al. 2007; Ebeling et al. 2014; Poggianti et al. 2017; Boselli et al. 2018; Jáchym et al. 2019; Roberts et al. 2021b; Edler et al. 2023; Souchereau et al. 2025). Moving forward it will be extremely valuable to obtain multi-phase observations of these high-redshift ram pressure tails to further understand this process in the early Universe and make detailed comparisons to examples at late times. There is also more marginal evidence for RPS at $z > 1$ in the literature, which has often been limited by angular resolution. Noble et al. (2019) present possible molecular gas extensions for cluster galaxies at $z \sim 1.6$, which may be tracing RPS. More indirect inferences have also been made in favor RPS in this redshift range (e.g. Nantais et al. 2017; Hamadouche et al. 2024), though in these cases it is more difficult conclusively associate the observed trends with specific quenching mechanisms.

7. CONCLUSIONS

² Here our discussion is primarily referring to galaxies ‘D4’, ‘D5’, and ‘D6’ from Xu et al. (2025) which seem to be the most compelling examples.

In this work we present COSMOS2020-635829 as a likely jellyfish galaxy undergoing ram pressure stripping at $z = 1.156$. Given the paucity of direct evidence for ram pressure stripping at $z > 1$, COSMOS2020-635829 is represents an important new addition to the broader understanding of environmental quenching at these early times. The key takeaways from this work are the following:

- COSMOS2020-635829 displays a symmetric stellar disk accompanied by a trail of star-forming knots to the south of the main galaxy, as identified from multi-band JWST imaging.
- We detect an ionized gas tail detected via the [OII] $\lambda\lambda 3726 - 3729$ doublet that is co-spatial with these extra-planar continuum sources.
- The star-forming knots in the tail have stellar masses of $\sim 10^8 M_{\odot}$ and SFRs of $\sim 0.3 M_{\odot} \text{ yr}^{-1}$, though it is possible that the values represent to totals for smaller knots below our resolution level that are being blended together. In total, these sources account for roughly 1% of the stellar mass and SFR of the main galaxy disk.

This work highlights the powerful combination of depth and angular resolution afforded by the *James Webb Space Telescope*. This permits spatially resolved analyses in order to directly constrain the quenching mechanisms at work in the high-redshift Universe. COSMOS2020-635829 is now an important laboratory in this regard and efforts moving forward will be dedicated to confirming the nature of this galaxy via multi-wavelength observations of the likely ram pressure tail presented in this work.

1 IDR acknowledges support from the Banting Fellowship
 2 Program. We thanks the COSMOS-Web team for pro-
 3 viding publicly available, science-ready data products.
 4 This work was enabled by observations made from the
 5 Gemini North telescope, located within the Maunakea
 6 Science Reserve and adjacent to the summit of Mau-
 7 nakea. We are grateful for the privilege of observing
 8 the Universe from a place that is unique in both its as-
 9 tronomical quality and its cultural significance. This
 10 work is based in part on observations obtained at the
 11 international Gemini Observatory, a program of NSF
 12 NOIRLab, which is managed by the Association of Uni-
 13 versities for Research in Astronomy (AURA) under a
 14 cooperative agreement with the U.S. National Science
 15 Foundation on behalf of the Gemini Observatory part-
 16 nership: the U.S. National Science Foundation (United
 17 States), National Research Council (Canada), Agencia
 18 Nacional de Investigación y Desarrollo (Chile), Minis-
 19 terio de Ciencia, Tecnología e Innovación (Argentina),
 20 Ministério da Ciência, Tecnologia, Inovações e Comu-
 21 nicações (Brazil), and Korea Astronomy and Space Sci-
 22 ence Institute (Republic of Korea). This work is based
 23 in part on observations made with the NASA/ESA/CSA
 24 James Webb Space Telescope. The data were obtained
 25 from the Mikulski Archive for Space Telescopes at the
 26 Space Telescope Science Institute, which is operated
 27 by the Association of Universities for Research in As-
 28 tronomy, Inc., under NASA contract NAS 5-03127 for
 29 JWST. This research is based in part on observations
 30 made with the NASA/ESA Hubble Space Telescope ob-
 31 tained from the Space Telescope Science Institute, which
 32 is operated by the Association of Universities for Re-
 33 search in Astronomy, Inc., under NASA contract NAS
 34 5–26555.

Facilities: Gemini:North (GMOS), HST (ACS),
 JWST (NIRCam), Subaru (Suprime-Cam)

Software: AstroPy (Astropy Collaboration et al.
 2013), Bagpipes (Carnall et al. 2018), Matplotlib (Hunter
 2007), Nautilus (Lange 2023), NumPy (Harris et al.
 2020)

REFERENCES

- Akerman, N., Tonnesen, S., Poggianti, B. M., et al. 2025,
 arXiv e-prints, arXiv:2504.11526,
 doi: [10.48550/arXiv.2504.11526](https://doi.org/10.48550/arXiv.2504.11526)
 Astropy Collaboration, Robitaille, T. P., Tollerud, E. J.,
 et al. 2013, A&A, 558, A33,
 doi: [10.1051/0004-6361/201322068](https://doi.org/10.1051/0004-6361/201322068)
 Balogh, M. L., Morris, S. L., Yee, H. K. C., Carlberg, R. G.,
 & Ellingson, E. 1999, ApJ, 527, 54, doi: [10.1086/308056](https://doi.org/10.1086/308056)
 Bellhouse, C., McGee, S. L., Smith, R., et al. 2021,
 MNRAS, 500, 1285, doi: [10.1093/mnras/staa3298](https://doi.org/10.1093/mnras/staa3298)
 Blanton, M. R., & Moustakas, J. 2009, ARAA, 47, 159,
 doi: [10.1146/annurev-astro-082708-101734](https://doi.org/10.1146/annurev-astro-082708-101734)

- Boselli, A., Fossati, M., & Sun, M. 2022, *A&AR*, 30, 3, doi: [10.1007/s00159-022-00140-3](https://doi.org/10.1007/s00159-022-00140-3)
- Boselli, A., & Gavazzi, G. 2006, *PASP*, 118, 517, doi: [10.1086/500691](https://doi.org/10.1086/500691)
- Boselli, A., Fossati, M., Ferrarese, L., et al. 2018, *A&A*, 614, A56, doi: [10.1051/0004-6361/201732407](https://doi.org/10.1051/0004-6361/201732407)
- Boselli, A., Epinat, B., Contini, T., et al. 2019, *A&A*, 631, A114, doi: [10.1051/0004-6361/201936133](https://doi.org/10.1051/0004-6361/201936133)
- Boselli, A., Lupi, A., Epinat, B., et al. 2021, *A&A*, 646, A139, doi: [10.1051/0004-6361/202039046](https://doi.org/10.1051/0004-6361/202039046)
- Broderick, A. O., Roberts, I. D., & Hudson, M. J. 2025, *arXiv e-prints*, arXiv:2505.10633, doi: [10.48550/arXiv.2505.10633](https://doi.org/10.48550/arXiv.2505.10633)
- Brown, T., Roberts, I. D., Thorp, M., et al. 2023, *ApJ*, 956, 37, doi: [10.3847/1538-4357/acf195](https://doi.org/10.3847/1538-4357/acf195)
- Bureau, M., & Carignan, C. 2002, *AJ*, 123, 1316, doi: [10.1086/338899](https://doi.org/10.1086/338899)
- Burke, C., Collins, C. A., Stott, J. P., & Hilton, M. 2012, *MNRAS*, 425, 2058, doi: [10.1111/j.1365-2966.2012.21555.x](https://doi.org/10.1111/j.1365-2966.2012.21555.x)
- Calzetti, D., Armus, L., Bohlin, R. C., et al. 2000, *ApJ*, 533, 682, doi: [10.1086/308692](https://doi.org/10.1086/308692)
- Carnall, A. C., Leja, J., Johnson, B. D., et al. 2019, *ApJ*, 873, 44, doi: [10.3847/1538-4357/ab04a2](https://doi.org/10.3847/1538-4357/ab04a2)
- Carnall, A. C., McLure, R. J., Dunlop, J. S., & Davé, R. 2018, *MNRAS*, 480, 4379, doi: [10.1093/mnras/sty2169](https://doi.org/10.1093/mnras/sty2169)
- Casey, C. M., Kartaltepe, J. S., Drakos, N. E., et al. 2023, *ApJ*, 954, 31, doi: [10.3847/1538-4357/acc2bc](https://doi.org/10.3847/1538-4357/acc2bc)
- Cerulo, P., Couch, W. J., Lidman, C., et al. 2016, *MNRAS*, 457, 2209, doi: [10.1093/mnras/stw080](https://doi.org/10.1093/mnras/stw080)
- Chung, A., van Gorkom, J. H., Kenney, J. D. P., & Vollmer, B. 2007, *ApJL*, 659, L115, doi: [10.1086/518034](https://doi.org/10.1086/518034)
- Copetti, M. V. F., & Writzl, B. C. 2002, *A&A*, 382, 282, doi: [10.1051/0004-6361:20011621](https://doi.org/10.1051/0004-6361:20011621)
- Cortese, L., Catinella, B., & Smith, R. 2021, *PASA*, 38, e035, doi: [10.1017/pasa.2021.18](https://doi.org/10.1017/pasa.2021.18)
- Cortese, L., Boissier, S., Boselli, A., et al. 2012, *A&A*, 544, A101, doi: [10.1051/0004-6361/201219312](https://doi.org/10.1051/0004-6361/201219312)
- Crossett, J. P., Jaffé, Y. L., McGee, S. L., et al. 2025, *A&A*, 694, A204, doi: [10.1051/0004-6361/202450371](https://doi.org/10.1051/0004-6361/202450371)
- de Propriis, R., Stanford, S. A., Eisenhardt, P. R., Dickinson, M., & Elston, R. 1999, *AJ*, 118, 719, doi: [10.1086/300978](https://doi.org/10.1086/300978)
- DESI Collaboration, Adame, A. G., Aguilar, J., et al. 2024, *AJ*, 168, 58, doi: [10.3847/1538-3881/ad3217](https://doi.org/10.3847/1538-3881/ad3217)
- Dressler, A. 1980, *ApJ*, 236, 351, doi: [10.1086/157753](https://doi.org/10.1086/157753)
- Durret, F., Chiche, S., Lobo, C., & Jauzac, M. 2021, *A&A*, 648, A63, doi: [10.1051/0004-6361/202039770](https://doi.org/10.1051/0004-6361/202039770)
- Ebeling, H., Stephenson, L. N., & Edge, A. C. 2014, *ApJL*, 781, L40, doi: [10.1088/2041-8205/781/2/L40](https://doi.org/10.1088/2041-8205/781/2/L40)
- Edler, H. W., de Gasperin, F., Shimwell, T. W., et al. 2023, *A&A*, 676, A24, doi: [10.1051/0004-6361/202346458](https://doi.org/10.1051/0004-6361/202346458)
- Ferland, G. J., Chatzikos, M., Guzmán, F., et al. 2017, *RMxAA*, 53, 385, doi: [10.48550/arXiv.1705.10877](https://doi.org/10.48550/arXiv.1705.10877)
- Finn, R. A., Desai, V., Rudnick, G., et al. 2018, *ApJ*, 862, 149, doi: [10.3847/1538-4357/aac32a](https://doi.org/10.3847/1538-4357/aac32a)
- Finn, R. A., Rudnick, G., Jablonka, P., et al. 2025, *The Astrophysical Journal*, 985, 81, doi: [10.3847/1538-4357/adc566](https://doi.org/10.3847/1538-4357/adc566)
- Foreman-Mackey, D., Hogg, D. W., Lang, D., & Goodman, J. 2013, *PASP*, 125, 306, doi: [10.1086/670067](https://doi.org/10.1086/670067)
- Franco, M., Casey, C. M., Koekemoer, A. M., et al. 2025, *arXiv e-prints*, arXiv:2506.03256, doi: [10.48550/arXiv.2506.03256](https://doi.org/10.48550/arXiv.2506.03256)
- Fumagalli, M., Gavazzi, G., Scaramella, R., & Franzetti, P. 2011, *A&A*, 528, A46, doi: [10.1051/0004-6361/201015463](https://doi.org/10.1051/0004-6361/201015463)
- Gavazzi, G. 1978, *A&A*, 69, 355
- Gavazzi, G., Boselli, A., Mayer, L., et al. 2001, *ApJL*, 563, L23, doi: [10.1086/338389](https://doi.org/10.1086/338389)
- Gavazzi, G., & Jaffe, W. 1987, *A&A*, 186, L1
- Gunn, J. E., & Gott, III, J. R. 1972, *ApJ*, 176, 1, doi: [10.1086/151605](https://doi.org/10.1086/151605)
- Haines, C. P., Pereira, M. J., Smith, G. P., et al. 2015, *ApJ*, 806, 101, doi: [10.1088/0004-637X/806/1/101](https://doi.org/10.1088/0004-637X/806/1/101)
- Hamadouche, M. L., McLure, R. J., Carnall, A., et al. 2024, *arXiv e-prints*, arXiv:2412.09592, doi: [10.48550/arXiv.2412.09592](https://doi.org/10.48550/arXiv.2412.09592)
- Harris, C. R., Millman, K. J., van der Walt, S. J., et al. 2020, *Nature*, 585, 357, doi: [10.1038/s41586-020-2649-2](https://doi.org/10.1038/s41586-020-2649-2)
- Hester, J. A., Seibert, M., Neill, J. D., et al. 2010, *ApJL*, 716, L14, doi: [10.1088/2041-8205/716/1/L14](https://doi.org/10.1088/2041-8205/716/1/L14)
- Hu, D., Zajaček, M., Werner, N., et al. 2024, *MNRAS*, 527, 1062, doi: [10.1093/mnras/stad3219](https://doi.org/10.1093/mnras/stad3219)
- Hunter, J. D. 2007, *Computing In Science & Engineering*, 9, 90, doi: [10.1109/MCSE.2007.55](https://doi.org/10.1109/MCSE.2007.55)
- Ignesti, A., Vulcani, B., Botteon, A., et al. 2023, *A&A*, 675, A118, doi: [10.1051/0004-6361/202346517](https://doi.org/10.1051/0004-6361/202346517)
- Jáchym, P., Kenney, J. D. P., Sun, M., et al. 2019, *ApJ*, 883, 145, doi: [10.3847/1538-4357/ab3e6c](https://doi.org/10.3847/1538-4357/ab3e6c)
- Jaffé, Y. L., Poggianti, B. M., Moretti, A., et al. 2018, *MNRAS*, doi: [10.1093/mnras/sty500](https://doi.org/10.1093/mnras/sty500)
- Jiménez-Teja, Y., Dupke, R. A., Lopes de Oliveira, R., et al. 2019, *A&A*, 622, A183, doi: [10.1051/0004-6361/201833547](https://doi.org/10.1051/0004-6361/201833547)
- Joo, H., & Jee, M. J. 2023, *Nature*, 613, 37, doi: [10.1038/s41586-022-05396-4](https://doi.org/10.1038/s41586-022-05396-4)
- Junais, Boissier, S., Boselli, A., et al. 2021, *A&A*, 650, A99, doi: [10.1051/0004-6361/202040185](https://doi.org/10.1051/0004-6361/202040185)
- Kimm, T., Somerville, R. S., Yi, S. K., et al. 2009, *MNRAS*, 394, 1131, doi: [10.1111/j.1365-2966.2009.14414.x](https://doi.org/10.1111/j.1365-2966.2009.14414.x)

- Kodama, T., & Arimoto, N. 1997, *A&A*, 320, 41, doi: [10.48550/arXiv.astro-ph/9609160](https://doi.org/10.48550/arXiv.astro-ph/9609160)
- Koekemoer, A. M., Faber, S. M., Ferguson, H. C., et al. 2011, *ApJS*, 197, 36, doi: [10.1088/0067-0049/197/2/36](https://doi.org/10.1088/0067-0049/197/2/36)
- Kormendy, J., Fisher, D. B., Cornell, M. E., & Bender, R. 2009, *ApJS*, 182, 216, doi: [10.1088/0067-0049/182/1/216](https://doi.org/10.1088/0067-0049/182/1/216)
- Lange, J. U. 2023, *MNRAS*, 525, 3181, doi: [10.1093/mnras/stad2441](https://doi.org/10.1093/mnras/stad2441)
- Larson, R. B., Tinsley, B. M., & Caldwell, C. N. 1980, *ApJ*, 237, 692, doi: [10.1086/157917](https://doi.org/10.1086/157917)
- Lin, Y.-T., & Mohr, J. J. 2004, *ApJ*, 617, 879, doi: [10.1086/425412](https://doi.org/10.1086/425412)
- Lora, V., Smith, R., Fritz, J., Pasquali, A., & Raga, A. C. 2024, *ApJ*, 969, 24, doi: [10.3847/1538-4357/ad3cda](https://doi.org/10.3847/1538-4357/ad3cda)
- Maier, C., Hayashi, M., Ziegler, B. L., & Kodama, T. 2019, *A&A*, 626, A14, doi: [10.1051/0004-6361/201935522](https://doi.org/10.1051/0004-6361/201935522)
- Mancone, C. L., Gonzalez, A. H., Brodwin, M., et al. 2010, *ApJ*, 720, 284, doi: [10.1088/0004-637X/720/1/284](https://doi.org/10.1088/0004-637X/720/1/284)
- Manuwal, A., & Stevens, A. R. H. 2023, *MNRAS*, 523, 2738, doi: [10.1093/mnras/stad1587](https://doi.org/10.1093/mnras/stad1587)
- Marleau, F. R., Cuillandre, J. C., Cantiello, M., et al. 2025, *A&A*, 697, A12, doi: [10.1051/0004-6361/202450799](https://doi.org/10.1051/0004-6361/202450799)
- Mayer, L., Mastropietro, C., Wadsley, J., Stadel, J., & Moore, B. 2006, *MNRAS*, 369, 1021, doi: [10.1111/j.1365-2966.2006.10403.x](https://doi.org/10.1111/j.1365-2966.2006.10403.x)
- McConnachie, A. W., Venn, K. A., Irwin, M. J., Young, L. M., & Geehan, J. J. 2007, *ApJL*, 671, L33, doi: [10.1086/524887](https://doi.org/10.1086/524887)
- McDonald, M., Allen, S. W., Bayliss, M., et al. 2017, *ApJ*, 843, 28, doi: [10.3847/1538-4357/aa7740](https://doi.org/10.3847/1538-4357/aa7740)
- Moretti, A., Radovich, M., Poggianti, B. M., et al. 2022, *ApJ*, 925, 4, doi: [10.3847/1538-4357/ac36c7](https://doi.org/10.3847/1538-4357/ac36c7)
- Morgan, C. R., Balogh, M. L., Boselli, A., et al. 2024, *A&A*, 691, A20, doi: [10.1051/0004-6361/202449225](https://doi.org/10.1051/0004-6361/202449225)
- Muzzin, A., Wilson, G., Yee, H. K. C., et al. 2012, *ApJ*, 746, 188, doi: [10.1088/0004-637X/746/2/188](https://doi.org/10.1088/0004-637X/746/2/188)
- Muzzin, A., van der Burg, R. F. J., McGee, S. L., et al. 2014, *ApJ*, 796, 65, doi: [10.1088/0004-637X/796/1/65](https://doi.org/10.1088/0004-637X/796/1/65)
- Nantais, J. B., Muzzin, A., van der Burg, R. F. J., et al. 2017, *MNRAS*, 465, L104, doi: [10.1093/mnrasl/slz224](https://doi.org/10.1093/mnrasl/slz224)
- Noble, A. G., Muzzin, A., McDonald, M., et al. 2019, *ApJ*, 870, 56, doi: [10.3847/1538-4357/aaf1c6](https://doi.org/10.3847/1538-4357/aaf1c6)
- Old, L. J., Balogh, M. L., van der Burg, R. F. J., et al. 2020, *MNRAS*, 493, 5987, doi: [10.1093/mnras/staa579](https://doi.org/10.1093/mnras/staa579)
- Owers, M. S., Hudson, M. J., Oman, K. A., et al. 2019, *The Astrophysical Journal*, 873, 52, doi: [10.3847/1538-4357/ab0201](https://doi.org/10.3847/1538-4357/ab0201)
- Peng, Y., Maiolino, R., & Cochrane, R. 2015, *Nature*, 521, 192, doi: [10.1038/nature14439](https://doi.org/10.1038/nature14439)
- Peng, Y.-j., Lilly, S. J., Kovač, K., et al. 2010, *ApJ*, 721, 193, doi: [10.1088/0004-637X/721/1/193](https://doi.org/10.1088/0004-637X/721/1/193)
- Poggianti, B. M., Fasano, G., Omizzolo, A., et al. 2016, *AJ*, 151, 78, doi: [10.3847/0004-6256/151/3/78](https://doi.org/10.3847/0004-6256/151/3/78)
- Poggianti, B. M., Moretti, A., Gullieuszik, M., et al. 2017, *ApJ*, 844, 48, doi: [10.3847/1538-4357/aa78ed](https://doi.org/10.3847/1538-4357/aa78ed)
- Poggianti, B. M., Gullieuszik, M., Tonnesen, S., et al. 2019, *MNRAS*, 482, 4466, doi: [10.1093/mnras/sty2999](https://doi.org/10.1093/mnras/sty2999)
- Postman, M., Franx, M., Cross, N. J. G., et al. 2005, *ApJ*, 623, 721, doi: [10.1086/428881](https://doi.org/10.1086/428881)
- Pradhan, A. K., Montenegro, M., Nahar, S. N., & Eissner, W. 2006, *MNRAS*, 366, L6, doi: [10.1111/j.1745-3933.2005.00119.x](https://doi.org/10.1111/j.1745-3933.2005.00119.x)
- Puchwein, E., Springel, V., Sijacki, D., & Dolag, K. 2010, *MNRAS*, 406, 936, doi: [10.1111/j.1365-2966.2010.16786.x](https://doi.org/10.1111/j.1365-2966.2010.16786.x)
- Quilis, V., Moore, B., & Bower, R. 2000, *Science*, 288, 1617, doi: [10.1126/science.288.5471.1617](https://doi.org/10.1126/science.288.5471.1617)
- Rasmussen, J., Ponman, T. J., & Mulchaey, J. S. 2006, *MNRAS*, 370, 453, doi: [10.1111/j.1365-2966.2006.10492.x](https://doi.org/10.1111/j.1365-2966.2006.10492.x)
- Roberts, I. D., & Parker, L. C. 2017, *MNRAS*, 467, 3268, doi: [10.1093/mnras/stx317](https://doi.org/10.1093/mnras/stx317)
- . 2020, *MNRAS*, 495, 554, doi: [10.1093/mnras/staa1213](https://doi.org/10.1093/mnras/staa1213)
- Roberts, I. D., Parker, L. C., Brown, T., et al. 2019, *ApJ*, 873, 42, doi: [10.3847/1538-4357/ab04f7](https://doi.org/10.3847/1538-4357/ab04f7)
- Roberts, I. D., van Weeren, R. J., de Gasperin, F., et al. 2024, *A&A*, 689, A22, doi: [10.1051/0004-6361/202450672](https://doi.org/10.1051/0004-6361/202450672)
- Roberts, I. D., van Weeren, R. J., McGee, S. L., et al. 2021a, *A&A*, 652, A153, doi: [10.1051/0004-6361/202141118](https://doi.org/10.1051/0004-6361/202141118)
- Roberts, I. D., van Weeren, R. J., Timmerman, R., et al. 2022a, *A&A*, 658, A44, <https://arxiv.org/abs/2112.08728>
- Roberts, I. D., van Weeren, R. J., McGee, S. L., et al. 2021b, *A&A*, 650, A111, doi: [10.1051/0004-6361/202140784](https://doi.org/10.1051/0004-6361/202140784)
- Roberts, I. D., Parker, L. C., Gwyn, S., et al. 2022b, *MNRAS*, 509, 1342, doi: [10.1093/mnras/stab3101](https://doi.org/10.1093/mnras/stab3101)
- Schaefer, A. L., Croom, S. M., Allen, J. T., et al. 2017, *MNRAS*, 464, 121, doi: [10.1093/mnras/stw2289](https://doi.org/10.1093/mnras/stw2289)
- Schaefer, A. L., Croom, S. M., Scott, N., et al. 2019, *MNRAS*, 483, 2851, doi: [10.1093/mnras/sty3258](https://doi.org/10.1093/mnras/sty3258)
- Sok, V., Muzzin, A., Jablonka, P., et al. 2022, *ApJ*, 924, 7, doi: [10.3847/1538-4357/ac2f40](https://doi.org/10.3847/1538-4357/ac2f40)
- Souchereau, H. J., Kenney, J. D. P., Jachym, P., et al. 2025, arXiv e-prints, arXiv:2506.07262, <https://arxiv.org/abs/2506.07262>
- Speagle, J. S., Steinhardt, C. L., Capak, P. L., & Silverman, J. D. 2014, *ApJS*, 214, 15, doi: [10.1088/0067-0049/214/2/15](https://doi.org/10.1088/0067-0049/214/2/15)

- Steinhauser, D., Schindler, S., & Springel, V. 2016, *A&A*, 591, A51, doi: [10.1051/0004-6361/201527705](https://doi.org/10.1051/0004-6361/201527705)
- Sun, M. 2012, *New Journal of Physics*, 14, 045004, doi: [10.1088/1367-2630/14/4/045004](https://doi.org/10.1088/1367-2630/14/4/045004)
- Toni, G., Maturi, M., Finoguenov, A., Moscardini, L., & Castignani, G. 2024, *A&A*, 687, A56, doi: [10.1051/0004-6361/202348832](https://doi.org/10.1051/0004-6361/202348832)
- Tonnesen, S., & Bryan, G. L. 2012, *MNRAS*, 422, 1609, doi: [10.1111/j.1365-2966.2012.20737.x](https://doi.org/10.1111/j.1365-2966.2012.20737.x)
- van der Burg, R. F. J., McGee, S., Aussel, H., et al. 2018, *A&A*, 618, A140, doi: [10.1051/0004-6361/201833572](https://doi.org/10.1051/0004-6361/201833572)
- Watts, A. B., Cortese, L., Catinella, B., et al. 2023, *PASA*, 40, e017, doi: [10.1017/pasa.2023.14](https://doi.org/10.1017/pasa.2023.14)
- Weaver, J. R., Kauffmann, O. B., Ilbert, O., et al. 2022, *ApJS*, 258, 11, doi: [10.3847/1538-4365/ac3078](https://doi.org/10.3847/1538-4365/ac3078)
- Wetzel, A. R., Tinker, J. L., & Conroy, C. 2012, *MNRAS*, 424, 232, doi: [10.1111/j.1365-2966.2012.21188.x](https://doi.org/10.1111/j.1365-2966.2012.21188.x)
- Wetzel, A. R., Tinker, J. L., Conroy, C., & van den Bosch, F. C. 2013, *MNRAS*, 432, 336, doi: [10.1093/mnras/stt469](https://doi.org/10.1093/mnras/stt469)
- Wilman, D. J., & Erwin, P. 2012, *ApJ*, 746, 160, doi: [10.1088/0004-637X/746/2/160](https://doi.org/10.1088/0004-637X/746/2/160)
- Xu, K., Wang, T., Daddi, E., et al. 2025, arXiv e-prints, arXiv:2503.21724, doi: [10.48550/arXiv.2503.21724](https://doi.org/10.48550/arXiv.2503.21724)
- Yagi, M., Yoshida, M., Komiyama, Y., et al. 2010, *AJ*, 140, 1814, doi: [10.1088/0004-6256/140/6/1814](https://doi.org/10.1088/0004-6256/140/6/1814)
- Yun, K., Pillepich, A., Zinger, E., et al. 2019, *MNRAS*, 483, 1042, doi: [10.1093/mnras/sty3156](https://doi.org/10.1093/mnras/sty3156)
- Zabel, N., Brown, T., Wilson, C. D., et al. 2022, *ApJ*, 933, 10, doi: [10.3847/1538-4357/ac6e68](https://doi.org/10.3847/1538-4357/ac6e68)

APPENDIX

A. TAIL SOURCE SIZE ESTIMATE

As an illustrative example, we will consider the source(s) in region 1 (see Fig. 1). This region clearly contains two sources resolved by the JWST images. To constrain source sizes (and determine whether or not these are simply point sources) we make a small cutout around the sources in region 1 and fit the flux map with the sum of two 2D Gaussian distributions. Fig. 9(top) shows the average FWHM source size³ for each of the four JWST filters. For reference we also plot λ/D corresponding to the diffraction limited PSF size. The sources are marginally resolved with FWHM sizes that are $\sim 1.5\text{--}3\times$ larger than the diffraction limited PSF. In Fig. 9(bottom) we plot ‘deconvolved sizes’ as a function of wavelength, where the deconvolved size is given by

$$\theta_{\text{deconv}} = \sqrt{\theta^2 - \theta_{\text{diff}}^2}, \quad (\text{A1})$$

where θ is the best-fit source FWHM and θ_{diff} is the diffraction limited FWHM. After ‘deconvolution’ all filters agree on a FWHM source size of $0.13'' \approx 1 \text{ kpc}$ corresponding to an effective radius of $\sim 500 \text{ pc}$. The deconvolution is only formally valid if the underlying source distribution is well described by a symmetric 2D Gaussian (i.e. Sérsic index of 0.5), but still provides an approximate estimate for the characteristic underlying source size.

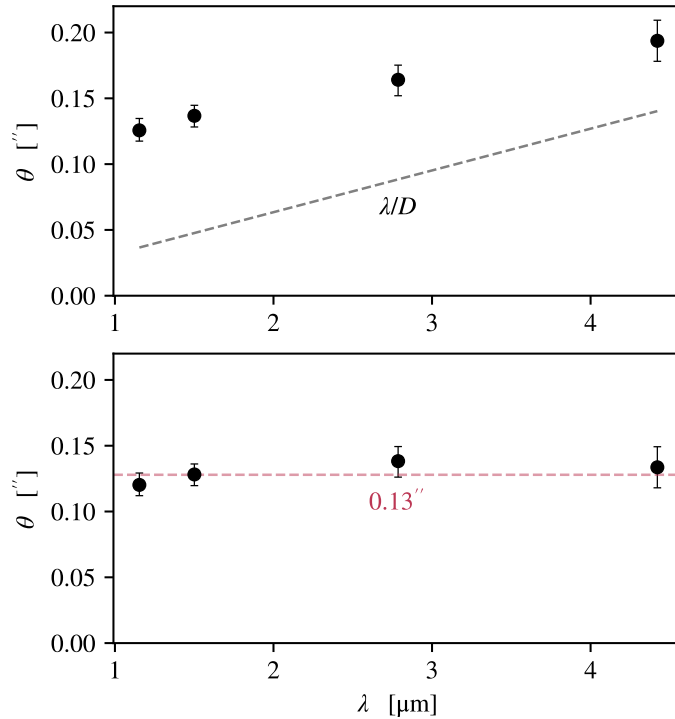


Figure 9. Size estimates for the extra-planar JWST sources in tail region 1. *Top:* Best-fit Gaussian FWHM size averaged over the two JWST sources in tail region 1. Data points correspond to the four JWST filters. For reference we show the diffraction-limited PSF FWHM as a function of wavelength (dashed line), indicating that these sources are only marginally resolved. *Bottom:* Deconvolved FWHM source sizes as a function of wavelength (see text for details).

³ The best-fit FWHMs for the two sources are consistent with each other for all filters, and therefore simplicity we only show the average FWHM.